Subpixel Mapping of Hyperspectral Images Using a Labeled-Unlabeled Hybrid Endmember Library and Abundance Optimization

Yifan Zhang, *Member, IEEE*, Ting Wang, Shaohui Mei, *Member, IEEE*, and Qian Du, *Fellow, IEEE*

***Abstract*—Classification at subpixel level for a low resolution hyperspectral image (LR HSI) is considered in this article. Using selected labeled samples as labeled endmembers and unsupervised clustering centers of LR HSI as unlabeled endmembers, a hybrid endmember library is constructed for spectral unmixing of LR HSI. The abundances of unlabeled endmembers are used to optimize the estimated fractional abundances of labeled classes within mixed pixels to improve the estimation accuracy. A more accurate subpixel mapping result is then obtained by applying subpixel spatial attraction model with the optimized fractional abundances. To incorporate spatial contextual information and further improve the subpixel mapping performance, a subpixel level segmentation map is generated by applying unsupervised clustering to the upsampled LR HSI, and integrated with the initial subpixel mapping result by decision fusion. Experimental results demonstrate that the proposed method remarkably outperforms state-of-the-art subpixel mapping methods, including the corresponding ones with or without spatial contextual information incorporation.**

***Index Terms*—Abundance, classification, endmember library, hyperspectral image (HSI), subpixel mapping.**

I. Introduction

HYPERSPECTRAL image (HSI) possesses hundreds of continuous spectral bands of observed objects, and provides abundant spectral information to improve the ability to distinguish different objects. As a result, it is widely used in classification [1], [2]. Meanwhile, due to the tradeoff between spatial and spectral resolution of hyperspectral sensors, the spatial resolution of HSI is usually limited, resulting in wide existence of mixed pixels. It is obvious that classic hard classification techniques, which assign a single class label to a pixel, are not appropriate. To address this issue, soft classification is used to estimate the proportion/probability of each class within a mixed pixel. More recently, spectral unmixing is also employed to decompose mixed pixels into several pure spectral constituents and quantitatively estimate their proportion [3].

Linear spectral mixture model [4] is usually employed to describe the spectral mixing behavior inside mixed pixels due to its simplicity and effectiveness. In spectral unmixing, endmembers play an important role in quantitatively representing spectral constituents of mixed pixels. Appropriate endmember extraction and selection from HSI is critical. Popular pure pixel based endmember extraction algorithms include pixel purity index [5], vertex component analysis [6], simplex growing algorithm [7], iterative error analysis [8], N-FINDR [9], etc. In cases with available training samples assigned to determined class labels, endmembers can also be selected from these training samples. In [10], an adaptive method is used to select the best endmember candidates from the training samples in the vicinity of a considered pixel. Unfortunately, the limited number of training samples for HSI is always a problem in practice, which greatly degrades accuracy of the following abundance estimation. Semisupervised classification methods [11]–[13] deal with the limited training samples by selecting informative unlabeled samples with active learning methods to enlarge the training sample set. Recently, novel feature extraction and unsupervised classification methods are also proposed to deal with the cases without any training samples [14]–[17].

Abundance fraction estimation following endmember extraction and selection also plays an important role in spectral unmixing. Fully constrained linear spectral unmixing (FCLSU) [18] and mixture-tuned matched filtering [19] are commonly used for abundance fraction estimation. As the linear mixing model generally satisfies two constraints: abundance sum-to-one constraint (ASC) and abundance nonnegative constraint (ANC) [20], abundance fractions can be interpreted as probabilities of endmember occurrence. By summing up abundance fractions of the endmembers (training samples) belonging to the same class, the proportion/probability of each class within the considered pixel (soft classification result) can be obtained.

Nevertheless, neither soft classification nor spectral unmixing is capable of providing any information about spatial distribution for each constituent/class within a mixed pixel. To account for this issue, subpixel mapping techniques are usually employed. The idea of subpixel mapping is originally proposed by Atkinson [21], which aims to arrange class spatial location inside each mixed pixel given their obtained abundances. Subpixel mapping techniques are employed for transforming an abundance map

Manuscript received June 27, 2019; revised February 27, 2020 and June 24, 2020; accepted July 16, 2020. Date of publication July 30, 2020; date of current version September 7, 2020. This work was supported by the National Natural Science Foundation of China under Grant 61420106007. *(Corresponding author: Yifan Zhang.)*

Yifan Zhang, Ting Wang, and Shaohui Mei are with the International Center for Information Acquisition and Processing, School of Electronics and Information, Northwestern Polytechnical University, Xi'an 710129, China (e-mail: yifanzhang@nwpu.edu.cn; 2369570597@qq.com; meish@nwpu.edu.cn).

Qian Du is with the Department of Electrical and Computer Engineering, Mississippi State University, Mississippi State, MS 39762 USA (e-mail: du@ece.msstate.edu).

Digital Object Identifier 10.1109/JSTARS.2020.3012982

into a finer classification map, according to abundance constraints (ASC and ANC) and spatial dependence [21] inspired by Tobler's first law [22]. The spatial dependence theory is implemented by the assumption that adjacent pixels most likely have the same class label. Many subpixel mapping techniques have been developed based on this theory, such as the direct neighboring subpixel mapping, the spatial attraction model [23]–[25], the pixel swapping subpixel mapping [26]–[29], the Hopfield neural network based techniques [30], [31], maximum *a posteriori*-based techniques [32]–[34], multiagent systems [35], genetic algorithms [36]–[38], differential evolution [39], etc. It has been illustrated that abundance map with higher accuracy normally leads to a finer subpixel mapping result [40].

In [41], taking a high resolution (HR) color image as auxiliary, a multisource subpixel mapping framework is exploited, and improved subpixel mapping results can be achieved by incorporating abundant and detailed spatial contextual information enclosed in the auxiliary image. However, this framework cannot be applied when there is no HR auxiliary image available [41], which is the most common case in practice. The collaborative representation based subpixel mapping (CRSPM) method proposed in [42] retains the two-branch structure in [41], while adopts the low-resolution HSI (denoted as LR HSI) as the only input. Two subpixel level classification maps are generated and fused by decision fusion to produce the final subpixel mapping result, one of which is achieved by classifying the upsampled LR HSI using collaborative representation-based (CR-based) classifier, the other is generated by using CR-based classification combined with spectral unmixing and subpixel spatial attraction model (SPSAM). Nevertheless, the adopted supervised classifier is quite critical to its performance. An advanced classifier usually results in better subpixel mapping result.

In this article, a new subpixel mapping method is proposed using the two-branch structure adopted by both [41] and [42], while taking the LR HSI as the only input. In one branch, an initial subpixel mapping result is produced by employing supervised classification, spectral unmixing, and SPSAM. Specifically, in spectral unmixing, a hybrid endmember library is constructed by using selected available labeled training samples as labeled endmembers and unsupervised clustering centers of LR HSI as unlabeled endmembers. The labeled abundances are optimized with the unlabeled ones to form a more accurate abundance map, so that the following SPSAM can produce a better subpixel mapping result. In the other branch, a segmentation map is generated by applying unsupervised clustering to the upsampled LR HSI. Results of these two branches are integrated by decision fusion to produce the final subpixel mapping result, incorporating spatial contextual information by using the segmentation map as a guide. Simulation experiments are employed to validate the correctness and effectiveness of the proposed method. Experimental results demonstrate its obvious outperformance over several state-of-the-art subpixel mapping methods by exhibiting less misclassification and better evaluation measurements. The comparison results also illustrate that the proposed method is less dependent on the employed supervised classifier, which can be attributed to introduction of the augmented hybrid endmember library incorporating both labeled and unlabeled endmembers as well as the following abundance optimization strategies adopted.

The remainder of this article is organized as follows. Section II provides a detailed description of the proposed subpixel mapping method. Section III shows the experimental results and analysis with different data sets. Section IV draws the conclusion.

II. Methodology

Framework of the proposed subpixel mapping method using hybrid endmember library and abundance optimization (HASPM method) is illustrated in Fig. 1. It is composed of three main parts: first, LR HSI subpixel mapping: Subpixel mapping is applied to the LR HSI to obtain an initial classification map at subpixel level. Second, HR segmentation: Unsupervised clustering is applied to the upsampled LR HSI (denoted as HR HSI) to obtain a segmentation map at subpixel level. Third, decision fusion: The obtained subpixel level segmentation map and initial classification map are combined with specific fusion strategy to generate the final subpixel level classification map.

The proposed HASPM method possesses the following main merits: first, the subpixel mapping result is obtained from a single LR HSI, without any auxiliary HR image (such as multispectral image or panchromatic image) available, which is a common case in practice. Second, to deal with the limited training samples (denoted as labeled endmembers in spectral unmixing) issue, unsupervised cluster centers are employed as unlabeled endmember to augment the endmember library to be a hybrid one. Meanwhile specific abundance optimization strategies are designed to improve the abundance estimation accuracy, which leads to improved subpixel mapping performance. Third, to incorporate spatial contextual information, segmentation map of the upsampled LR HSI is employed as a guideline for final subpixel mapping decision, based on the fact that spatially and spectrally close samples are more likely to belong to the same class.

A. LR HSI Subpixel Mapping

In this part, an initial classification map at subpixel level is produced by SPSAM based subpixel mapping, with abundance fractions estimated using specifically designed hybrid endmember library and corresponding abundance optimization strategies. For convenience, this part is denoted as InHASPM method.

1) Supervised Classification: An LR classification map is obtained by applying supervised classification to LR HSI, which provides a reference for endmember selection in the following spectral unmixing. Theoretically, any supervised classifiers can be adopted. For the purpose of validation and comparison without losing generality, two commonly used representative classifiers, support vector machine (SVM) and joint collaborative representation (JCR)-based classifiers, are adopted.

Initially, the objective of a binary SVM is to search for an optimal hyperplane that separates the feature space into two classes [43]. While the training set is usually nonlinearly separable in practice, an effective way is to project them onto another

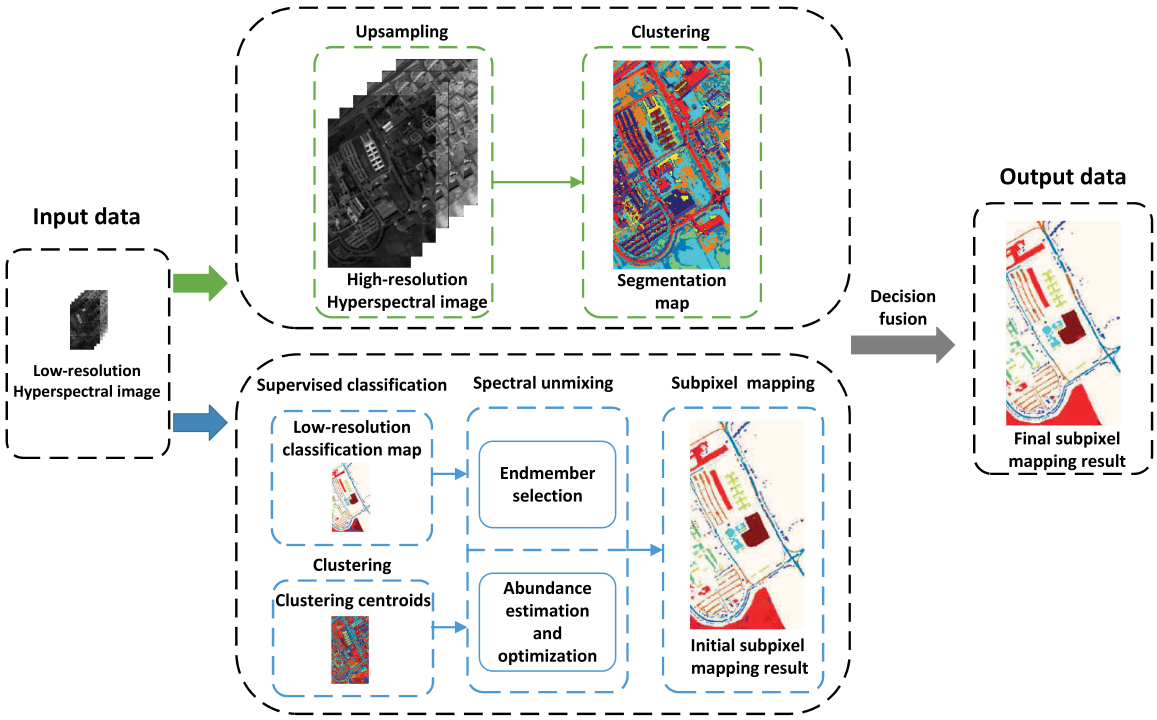

Fig. 1. Framework of the proposed subpixel mapping method.

higher dimensional space through a positive definite kernel [44], to acquire extended multiple-class classifier [45], [46].

Recently, it has been argued that it is the collaborative nature of atoms rather than competitive nature imposed by sparseness constraint that actually improves the classification accuracy. Thus, CR-based classifiers were developed for HSI classification for their better classification performance with much lower computational cost than the previous sparse representation based ones. The pixel-wise CR-based classifier using nearest regularized subspace (NRS) is proposed in [47]. To incorporate the spatial contextual information during classification, the spatially joint version of NRS, i.e., JCR, is proposed in [48] by considering neighboring test and labeled samples, and improved classification results can be acquired. The classifier using collaborative representation with Tikhonov regularization (CRT) is proposed in [48]. The essential difference between NRS and CRT is that the former employs within-class training samples for collaborative representation (also called prepartitioning) while the latter uses all the training data from different classes simultaneously (also called postpartitioning). It has been demonstrated that postpartitioning is more appropriate, particularly in the kernel-induced feature space [48]. To further improve the classification accuracy, CRT is extended to the spatially joint version (JCRT) by incorporating spatial contextual information [42]. It is notable that both CRT and JCRT based classifiers are more time-consuming than JCR-based classifier. To maintain a balance between classification accuracy and computational cost, JCR-based classifier is adopted in this work.

2) Spectral Unmixing: In this article, linear spectral mixing model (LMM) is adopted to describe the spectral mixing behavior of endmembers within mixed pixels. The spectral signature

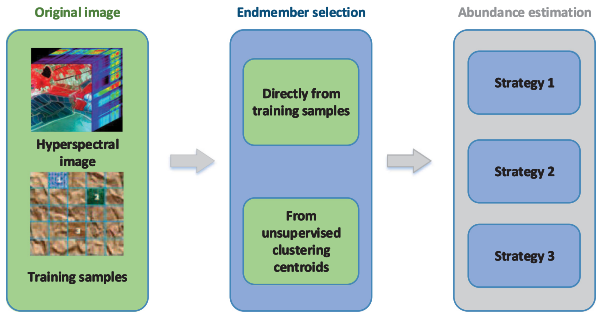

Fig. 2. Spectral unmixing with a hybrid endmember library and different abundance optimization strategies.

of a mixed pixel is represented with a linear combination of endmember spectral signatures. It is adopted for the following reasons: first, LMM is simple with clear physical meaning and is easy to be applied. Second, in most cases, LMM is capable of better approximating the spectral mixing behavior in a real scene with satisfactory accuracy for practical application requirements.

The obtained fractional abundances are used as the input for the following SPSAM to produce the initial subpixel mapping result. Since, it has been illustrated that abundance map with higher accuracy normally leads to a finer subpixel mapping result [40], more accurately estimated abundances are highly expected. Fig. 2 depicts the spectral unmixing scheme adopted in this article, which employs a hybrid endmember library and different abundance optimization strategies.

Labeled training samples are the most credible endmember candidates, which accurately describe spectral properties of land

TABLE I
ENDMEMBERS AND CORRESPONDING ABUNDANCES

	Labeled endmember				Unlabeled endmember			
Endmember	$\mathbf{x}_1$	$\mathbf{x}_2$	$\cdots$	$\mathbf{x}_N$	$\mathbf{y}_1$	$\mathbf{y}_2$	$\cdots$	$\mathbf{y}_K$
Abundance	$\boldsymbol{\alpha}_1$	$\boldsymbol{\alpha}_2$	$\cdots$	$\boldsymbol{\alpha}_N$	$\boldsymbol{\beta}_1$	$\boldsymbol{\beta}_2$	$\cdots$	$\boldsymbol{\beta}_K$

cover classes. While in practice, the available labeled training sample set usually exhibits limitation in both quantity and diversity, which greatly affects the accuracy of abundance estimation. Considering their good performance as global representatives, cluster centers of the LR HSI are also employed to serve as endmembers. Therefore, a hybrid endmember library is constructed, with selected labeled training samples as labeled endmembers and unsupervised cluster centers as unlabeled endmembers.

To mitigate spectral variability, N training samples spatially closet to a testing sample $\mathbf{z}$, instead of the entire labeled training sample set, are selected to form labeled endmember set $\mathbf{X} = \{\mathbf{x}_1, \mathbf{x}_2, \ldots, \mathbf{x}_N\}$. LR HSI is unsupervisedly clustered to K clusters, and all the K cluster centers serve as unlabeled endmembers to form the unlabeled endmember set $\mathbf{Y} = \{\mathbf{y}_1, \mathbf{y}_2, \ldots, \mathbf{y}_K\}$. Thus, the labeled-unlabeled hybrid endmember matrix for $\mathbf{z}$ becomes $[\mathbf{X}, \mathbf{Y}]$.

The FCLSU algorithm is employed to estimate abundance for each endmember depicted in Table I. Different labeled endmembers may belong to the same class. The labeled abundance of each class within the considered mixed pixel $\mathbf{z}$ can be obtained by summing up abundances of labeled endmembers sharing the same class label:

$$P_i = \sum_{j \in J} \boldsymbol{\alpha}_j, J = \{j | \text{class}(\mathbf{x}_j) = i\} \tag{1}$$

with $i = \{1, 2, \ldots, C\}$ and C is the number of land cover classes.

It is notable that, unlike labeled endmembers, there is no one-to-one relation between unlabeled endmembers (cluster centers) and land cover classes. The informative unlabeled endmembers, which can hardly be pure material, can be represented by labeled ones with LMM, so that the unlabeled abundances can be used to optimize fractional abundances. Three optimization strategies are proposed in this article.

Strategy 1: The abundance of each class within a mixed pixel can be regarded as the probability of the class to appear within the mixed pixel. The higher the abundance of a class, the more likely this class appears within the mixed pixel. In this strategy, all the unlabeled endmembers are categorized to the class with the highest labeled abundance, that is the class most likely to appear. The optimized abundance for class i in the mixed pixel is then calculated as follows:

$$\widetilde{P}_i = \begin{cases} P_i + \sum_k \boldsymbol{\beta}_k, & i = \arg\max_c P_c \\ P_i, & \text{others.} \end{cases} \tag{2}$$

Strategy 2: As abovementioned, unlabeled endmember is hardly pure material, and is composed of different labeled endmembers. It is appropriate to assume that within a given mixed pixel, unlabeled endmembers share the same class abundance distribution as labeled endmembers. This leads to the following abundance optimization strategy, in which the unlabeled abundance is proportionally added to labeled abundance of each class. The abundance can then be optimized as follows:

$$\widetilde{P}_i = P_i + \sum_k \frac{P_i}{P} \boldsymbol{\beta}_k \text{ with } P = \sum_i P_i. \tag{3}$$

Strategy 3: As mentioned in Strategy 1, lower labeled abundance of a class implies less occurrence probability. For example, classes with labeled abundance less than $1/S^2$ (S^2 is the number of subpixels within a mixed pixel), denoting proportion of those classes within the mixed pixel is less than one subpixel, are less likely to appear. Therefore, a threshold ζ is set in this strategy to keep the small labeled abundances unchanged. The abundance optimization is applied as follows:

$$\widetilde{P}_i = \begin{cases} P_i + \sum_k \frac{P_i \cdot \boldsymbol{\beta}_k}{\sum_{j \in J} P_j}, & P_i \geq \zeta, J = \{j | P_j \geq \zeta\} \\ P_i, & P_i < \zeta \end{cases} \tag{4}$$

where ζ is the predefined threshold within [0, 1].

3) Subpixel Mapping: For a given mixed pixel, fractional abundances for land cover classes within it are obtained by spectral unmixing, whereas the physical distribution of classes within it is still unknown. Subpixel mapping is capable of dealing with this issue by predicting the location of all class labels within a mixed pixel [21]. To accomplish the rearrangement, most subpixel mapping algorithms (such as genetic algorithms, algorithms using neural networks, and simulated annealing) adopt iterative strategies, which are computationally expensive. SPSAM-based subpixel mapping algorithm directly estimates subpixel classes according to the class proportions in neighboring pixels without any random initialization [25]. It is adopted in this work for its simplicity and good performance. The basic assumption of SPSAM-based subpixel mapping algorithm is spatial dependence, as proposed by Atkinson in [21], which refers to the tendency for spatially approximate observations of a given property to be more alike than distant observations. To quantify this spatial dependence, attraction value between a subpixel within a coarse pixel and its eight neighboring coarse pixels is calculated. After attraction value calculation, subpixels are assigned to different classes according to the criterion that subpixels with highest attractions are first assigned [21].

B. HR Segmentation

To extract spatial contextual information, unsupervised clustering is applied to the upsampled LR HSI, that is the artificial HR HSI, to acquire a segmentation map. One coarse pixel in LR HSI is supposed to be divided into S^2 subpixels, as a result, LR HSI is spatially upsampled by a spatial scale factor S to

form the corresponding HR HSI. Then, unsupervised clustering is applied to it. In the obtained unsupervised clustering result, neighboring pixels with the same numerical label makes up a segment. It is notable that the size of segment (number of pixels enclosed in a segment) should be small enough, so that pixels inside a segment can better exhibit local spectral similarity and spatial proximity. Thus, the number of clusters should be greater than or equal to that of actual land cover classes in the observed scene.

C. Decision Fusion

There are two inputs at subpixel level for decision fusion: a segmentation map and an initial classification map. A specific fusion strategy is designed to incorporate spatial contextual information for accuracy improvement. Modification is applied to the initial classification map using the segmentation map at subpixel level as a guide, complying with the principle that subpixels within a segment share the same class label, while training samples always retain their original class labels. This principle is based on the fact that spatially and spectrally close subpixels are most likely belonging to the same land cover class. The detailed fusion rules are as following. First, subpixels enclosed within training samples remained their original class labels. Second, other subpixels are assigned with the class label which most frequently occurs within the segment they belong to.

III. Experimental Results and Analysis

A. Data Sets and Experimental Setup

Simulation is employed in this article. The original HSI (HR HSI) is downsampled with a spatial scale factor S to generate a LR HSI, to which subpixel mapping is applied. By applying subpixel mapping, each coarse pixel in LR HSI is divided into S^2 subpixels, and a unique class label is allocated to each subpixel to obtain a classification map in subpixel level. The ground truth of the original HSI serves as a reference to evaluate the subpixel mapping performance. To validate the proposed method and make a comparison with some state-of-the-art methods, objective measurements are also employed besides subjective assessment, including overall accuracy (OA) and kappa coefficient (κ), as well as the averaged producer accuracy (APA) and user accuracy (AUA) over all classes.

Two widely used HSI data sets collected by different hyperspectral imagery sensors are employed for simulation. The first data set (Indian Pines data set) was gathered by the airborne visible infrared imaging spectrometer (AVIRIS) over the Indian Pines test site in north-western Indiana and consists of 224 spectral reflectance bands in the wavelength range 400–2500 nm with 145×145 pixels in each band. The Indian Pines scene contains two-thirds agriculture, and one-third forest or other natural perennial vegetation. The data set is designated into 16 classes and is not all mutually exclusive. The number of bands is reduced to 202 by removing water-absorption bands, and 144×144 pixels are retained within each band for the purpose of calculation convenience.

The second data set (Pavia University data set) was gathered by the reflective optics system imaging spectrometer (ROSIS) over the urban area of University of Pavia, northern Italy and consists of 115 spectral reflectance bands in the wavelength range 430–860 nm with 610×340 pixels in each band. Ninth classes of interest are considered. The number of bands is reduced to 103 by removing the noisy ones, and 609×339 pixels are retained within each band for calculation convenience.

The ground reference data are also downsampled with the spatial scale factor S as well, to select pure pixels (i.e., coarse pixels within which all original subpixels belong to the same class) as the training samples. The spatial scale factor S is critical because inappropriate (normally too high) S may raise the danger of lacking training samples for some classes in LR HSI. It is obvious that the higher S is, the less training samples exist.

For Indian Pines data set, there is no pure coarse pixel in LR HSI for the ninth class (Oats) when $S = 3$, leading to unavailability of training samples for the ninth class. And S greater than three causes absence of pure coarse pixels (training samples) for even more classes. For Pavia University data set, $S = 4$ has already caused absence of pure coarse pixels (training samples) for several classes. To apply effective experiments without loss of generality, S is set to be 2 for Indian Pines data set and 3 for Pavia University data set. For Indian Pines data set, after downsampling with a spatial scale factor $S = 2$, 2213 pure pixels remain, 15% of which are used as training samples, that is, 333 training coarse pixels. For Pavia University data set, after downsampling with a spatial scale factor $S = 3$, only 206 pure pixels remain, all of which are employed to form the training set.

Specifically, for the proposed HASPM method, to acquire the HR HSI used in segmentation, the LR HSI is upsampled using cubic interpolation with the spatial scale factor S. As for unsupervised clustering involved, the classic K-means clustering is employed.

B. Parameter Settings

1) Number of Clusters: For LR HSI K-means clustering, the number of clusters K_1 represents the number of unlabeled endmembers. These unlabeled endmembers (clustering centers) are used to optimize the acquired fractional abundances of labeled endmembers. Theoretically, K_1 could be any positive integer. While the clusters are inconsistent with land cover classes, there is no one-to-one relationship between class labels and cluster centers. Thus, given the spectral variation and the difference of pixel numbers within different land cover classes, the value of K_1 should be larger than the number of actual land cover classes. Fig. 3(a) depicts OA of the proposed InHASPM method with varied K_1. OA exhibits an increase as K_1 increases for small K_1 and no salient changes after K_1 reaches around 20. Considering the high computation complexity with increasing K_1, without losing generality, $K_1 = 19$ for Indian Pines data set and $K_1 = 18$ for Pavia University data set in the following experiment.

For HR HSI, K-means clustering is applied to produce a segmentation map, which is used to fine-tune the acquired initial subpixel mapping result in decision fusion. The number of clusters K_2 represents the number of segments. The selection of

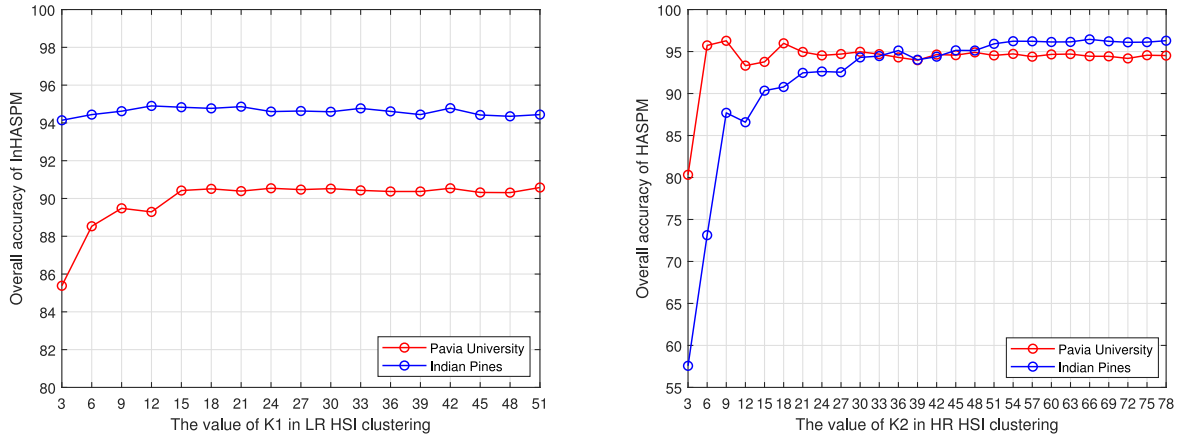

Fig. 3. Number of cluster center settings. (a) LR HSI clustering. (b) HR HSI clustering.

TABLE II
OA (%) WITH DIFFERENT ζ

Indian Pines data set											
ζ	0	0.1	0.2	0.3	0.4	0.5	0.6	0.7	0.8	0.9	1.0
S3-InHASPM	94.94	94.98	95.03	95.00	94.95	95.03	95.03	95.07	95.05	95.03	94.96
S3-HASPM	96.02	96.05	96.07	96.10	96.09	96.15	96.15	96.12	96.11	96.07	96.09
Pavia University data set											
ζ	0	0.1	0.2	0.3	0.4	0.5	0.6	0.7	0.8	0.9	1.0
S3-InHASPM	89.94	90.05	90.12	90.34	90.66	90.54	90.50	90.46	90.55	90.27	90.11
S3-HASPM	96.28	96.28	96.29	96.30	96.31	96.31	96.31	96.30	96.31	96.30	96.30

K_2 generally depends on the spatial distribution of land cover classes in HSI, which is normally unknown in practical applications. Therefore, K_2 is usually decided empirically. Fig. 3(b) depicts OA of the proposed HASPM method with varied K_2. It can be observed that excellent performance can be obtained with K_2 big enough, and no salient performance differences can be observed with K_2 big enough. Furthermore, for Pavia University data set, optimal performance can be obtained when K_2 is around 9, which is the number of actual land cover classes. The reason might be that in the ground truth of Pavia University scene, areas belonging to the same land cover class are distributed in a relatively connected manner. While for Indian Pines data set, in which the areas with the same class label may distribute in blocks within unconnected regions, K_2 should be much higher than the number of actual land cover classes. Considering the high computation complexity with increasing K_2, $K_2 = 9$ (the exact number of actual land cover classes) for Pavia University data set and $K_2 = 51$ (approximate to the number of disconnected blocks) for Indian Pines data set are employed in the following experiments.

It is notable that each run of K-means clustering for LR HSI and HR HSI may lead to different results, which affects subpixel mapping performance of both InHASPM and HASPM methods. Therefore, mean accuracy for ten different runs are calculated and displayed in the experiment.

2) Threshold ζ: In fractional abundance optimization Strategy 3, threshold ζ is introduced to determine which abundance fractions should be modified (the ones not less than ζ). With a wide range of experiments, it is found out that satisfied results with little differences can be obtained when the threshold ζ varying within the range of [0, 1]. OA of InHASPM and HASPM methods using Strategy 3 with varied ζ is shown in Table II. In the following experiments, without loss of generality, ζ is set to be 0.5 for both data sets.

C. Validation Experiment

For the purpose of validation, the proposed subpixel mapping framework is compared with different supervised classifiers (SVM-based classifier and JCR-based classifier) as well as different abundance optimization strategies (Strategy 1–3) using both ROSIS Pavia University data set and AVIRIS Indian Pines data set. The corresponding subpixel mapping results and values of evaluation measurements are depicted in Figs. 4–7 and Tables III–VI, in which S1, S2, and S3 represent Strategy 1, 2, and 3 respectively. It can be observed that the three different strategies produce comparable performance. In Strategy 1, unlabeled endmembers are directly assigned to the most probable class. In Strategy 2, unlabeled endmembers are proportionally assigned to all probable classes. Different from Strategy 2, Strategy 3 proportionally assigns unlabeled endmembers to several most probable classes rather than all probable classes. Meanwhile, it is worth noting that when threshold $\zeta = 0$, Strategy 3 is the same as Strategy 2. Strategy 2 and 3 are more theoretically reliable by emphasizing more probable classes, while since Strategy 1–3 exhibit no salient difference in performance,

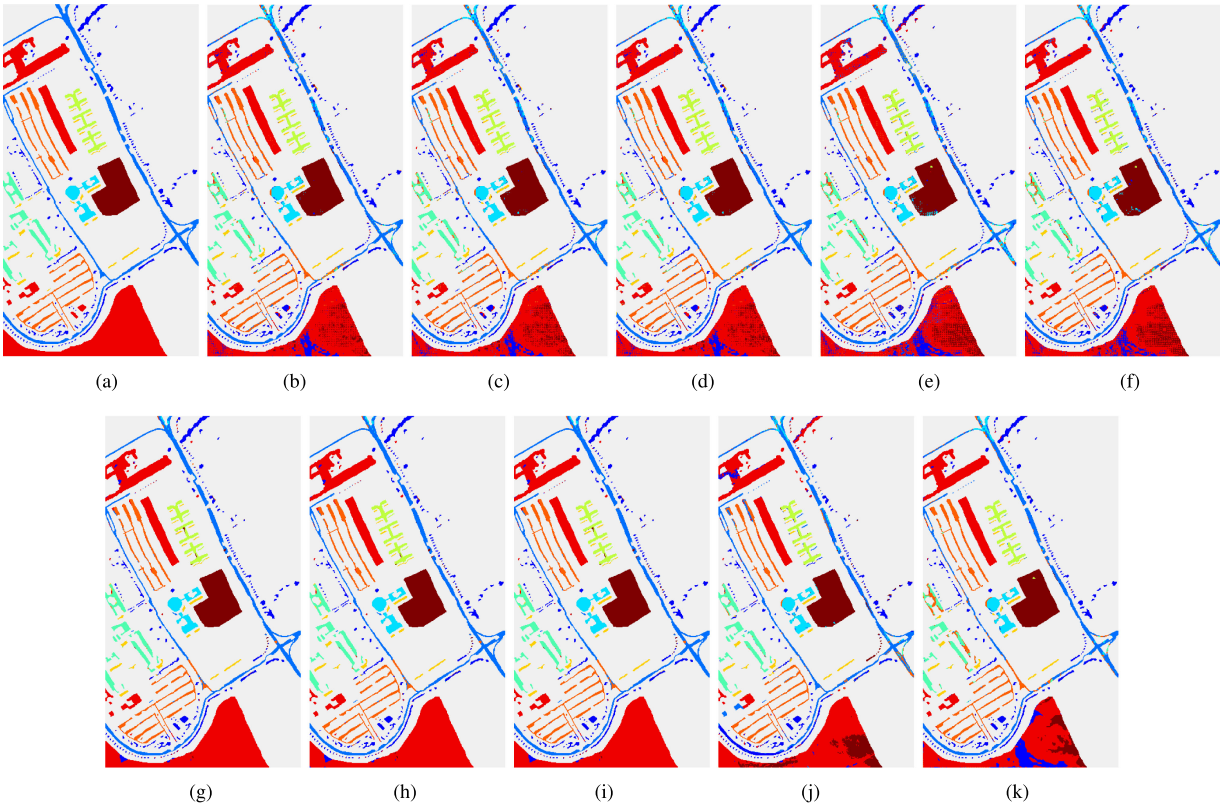

Fig. 4. Subpixel mapping results of different methods on Pavia University data set with SVM-based classifier. (a) Reference. (b) S1-InHASPM. (c) S2-InHASPM. (d) S3-InHASPM. (e) ASPM. (f) JASPM. (g) S1-HASPM. (h) S2-HASPM. (i) S3-HASPM. (j) ACSPM. (k) CRSPM.

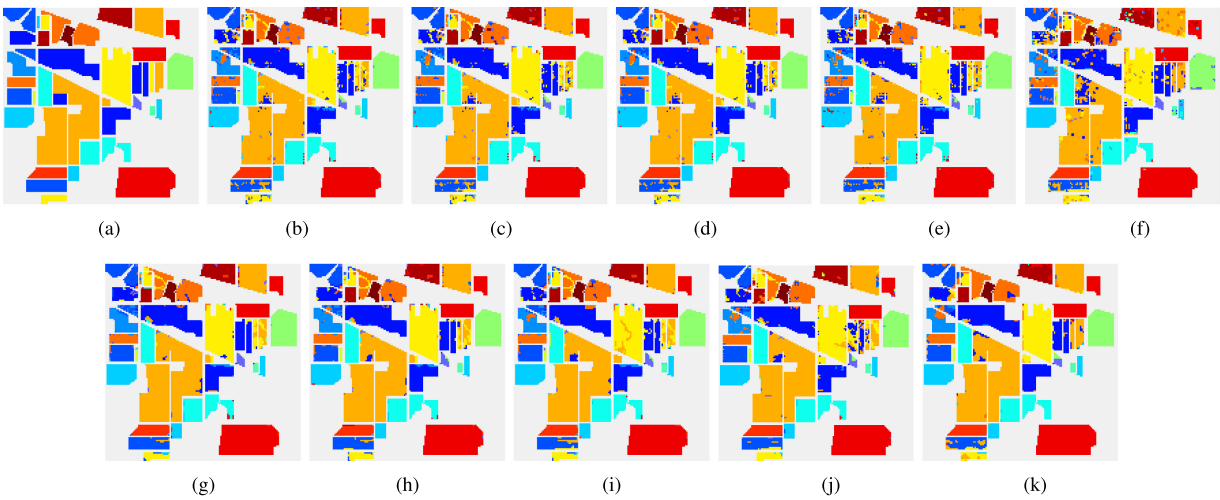

Fig. 5. Subpixel mapping results of different methods on Indian Pines data set with SVM-based classifier. (a) Reference. (b) S1-InHASPM. (c) S2-InHASPM. (d) S3-InHASPM. (e) ASPM. (f) JASPM. (g) S1-HASPM. (h) S2-HASPM. (i) S3-HASPM. (j) ACSPM. (k) CRSPM.

Strategy 1 is more preferable in practice for its calculation simplicity.

D. Comparison Experiment

The proposed framework is also compared with several state-of-the-art subpixel mapping methods, including the attraction based subpixel mapping (ASPM) and attraction based contextual subpixel mapping (ACSPM) methods developed in [41], as well as spatially joint attraction based subpixel mapping (JASPM) and CRSPM methods developed in [42]. In the ASPM method, the LR classification map is first obtained from the LR HSI using SVM classifier, for the purpose of endmember selection (to construct a labeled endmember library). Each mixed pixel

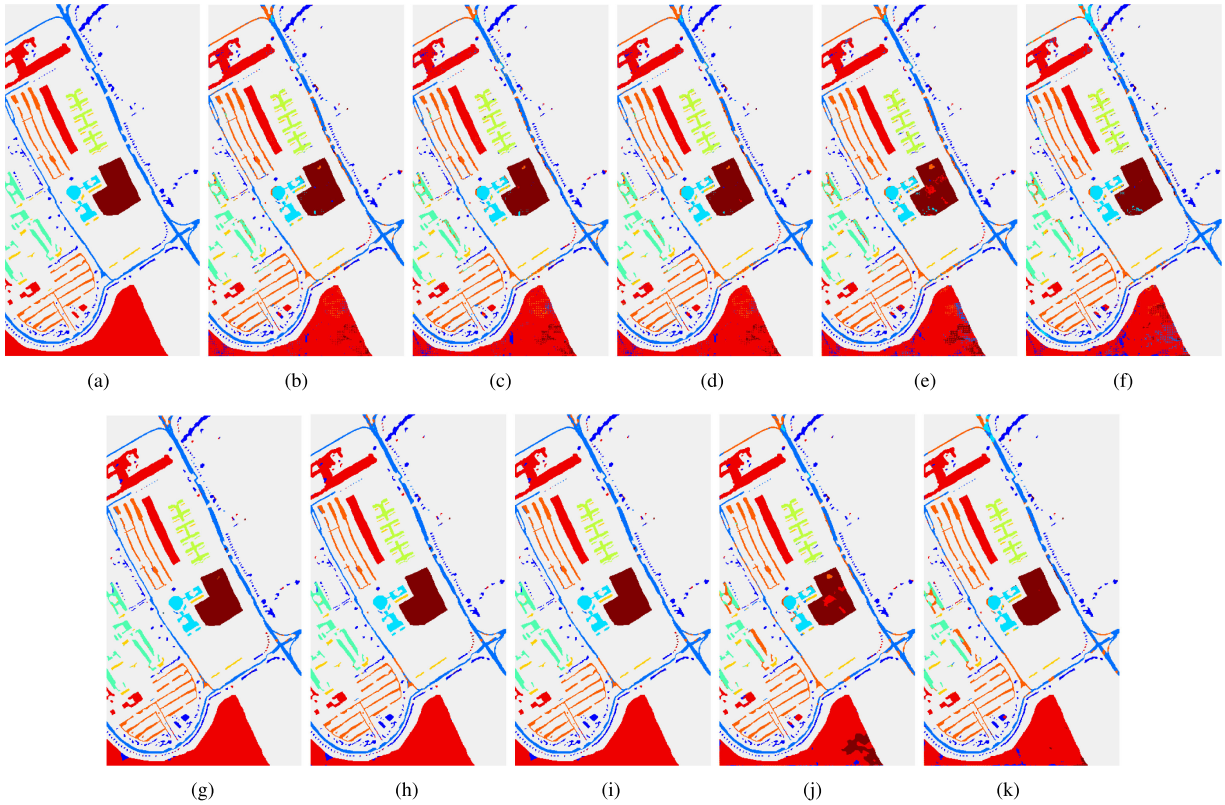

Fig. 6. Subpixel mapping results of different methods on Pavia University data set with JCR-based classifier. (a) Reference. (b) S1-InHASPM. (c) S2-InHASPM. (d) S3-InHASPM. (e) JASPM. (f) JASPM-JCRT. (g) S1-HASPM. (h) S2-HASPM. (i) S3-HASPM. (j) CRSPM. (k) CRSPM-JCRT.

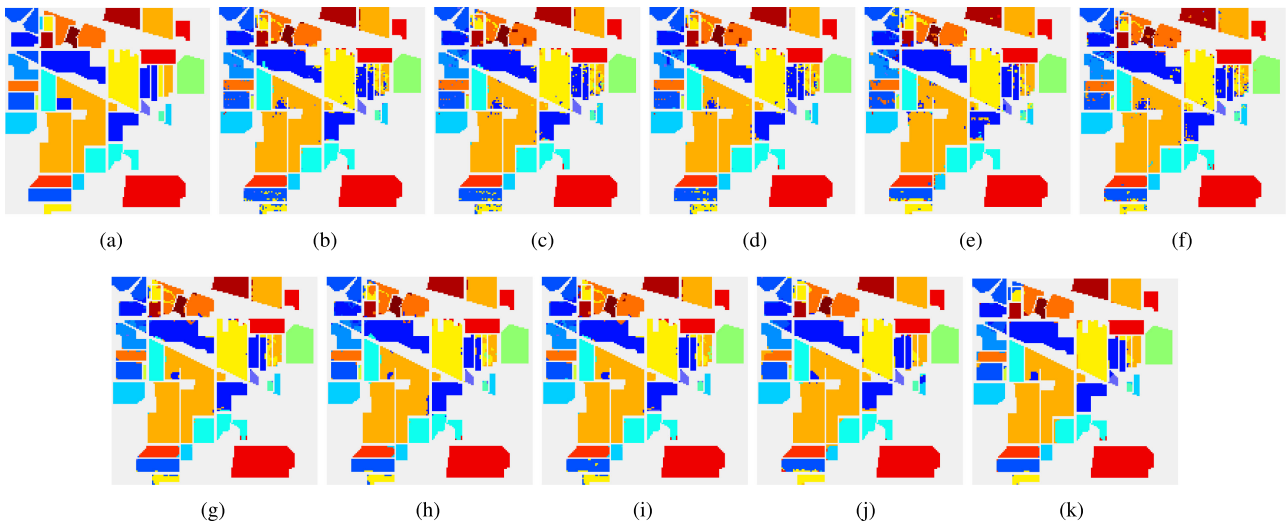

Fig. 7. Subpixel mapping results of different methods on Indian Pines data set with JCR-based classifier. (a) Reference. (b) S1-InHASPM. (c) S2-InHASPM. (d) S3-InHASPM. (e) JASPM. (f) JASPM-JCRT. (g) S1-HASPM. (h) S2-HASPM. (i) S3-HASPM. (j) CRSPM. (k) CRSPM-JCRT.

is then unmixed by spectral unmixing, to acquire abundance of each class within it. Finally, the SPSAM is employed to produce the subpixel mapping result. ACSPM method is composed of two parallel branches integrated by decision fusion: ASPM method and unsupervised clustering of a complementary HR color image. The major contribution of the ACSPM method should be the inclusion of contextual information obtained from the color image. However, just as mentioned in [41], the ACSPM framework relies heavily on the availability of a multisource data set. When no additional source of information (such as an HR color image) is available, it cannot be applied at all.

TABLE III
PERFORMANCE EVALUATION MEASUREMENTS OF DIFFERENT METHODS ON PAVIA UNIVERSITY DATA SET WITH SVM-BASED CLASSIFIER

Overall performance of one-branch methods					
Measurement	S1-InHASPM	S2-InHASPM	S3-InHASPM	ASPM	JASPM
OA[%]	**87.90**	86.72	87.58	81.36	84.70
κ	**0.844**	0.830	0.840	0.765	0.805
APA[%]	**90.16**	89.71	90.11	86.14	87.72
AUA[%]	**84.16**	83.09	83.94	78.92	82.33
Time(s)	143.17	142.95	143.21	**92.73**	109.71
Overall performance of two-branch methods					
Measurement	S1-HASPM	S2-HASPM	S3-HASPM	ACSPM	CRSPM
OA[%]	**96.67**	96.59	96.63	83.90	86.85
κ	**0.956**	0.955	**0.956**	0.793	0.833
APA[%]	**95.65**	95.53	95.59	86.39	89.90
AUA[%]	**95.26**	95.02	95.16	83.81	85.83
Time(s)	171.84	171.79	171.88	**97.61**	124.32

The bold entities indicate the best results and the underlined entities indicate the second best results.

TABLE IV
PERFORMANCE EVALUATION MEASUREMENTS OF DIFFERENT METHODS ON INDIAN PINES DATA SET WITH SVM-BASED CLASSIFIER

Overall performance of one-branch methods					
Measurement	S1-InHASPM	S2-InHASPM	S3-InHASPM	ASPM	JASPM
OA[%]	91.93	92.20	**92.33**	90.98	86.60
κ	0.908	0.911	**0.913**	0.897	0.847
APA[%]	89.51	89.95	**90.04**	88.64	87.18
AUA[%]	88.06	**88.31**	88.09	87.27	82.60
Time(s)	43.91	44.03	43.98	**21.38**	21.84
Overall performance of two-branch methods					
Measurement	S1-HASPM	S2-HASPM	S3-HASPM	ACSPM	CRSPM
OA[%]	94.01	**94.38**	93.40	92.70	92.97
κ	0.932	**0.936**	0.925	0.917	0.920
APA[%]	92.76	**93.22**	92.63	92.68	91.60
AUA[%]	90.19	90.76	88.39	90.36	**91.56**
Time(s)	71.80	71.66	71.91	**22.42**	28.39

The bold entities indicate the best results and the underlined entities indicate the second best results.

The CRSPM method in [42] is composed of three parts: JASPM method, spatially joint collaborative representation based high resolution hyperspectral image classification (JHHS) method, and decision fusion. The JASPM method produces a subpixel mapping result as ASPM method, while employing a specifically designed spatially joint and post-partitioning CR-based classifier (JCRT-based classifier) rather than SVM-based classifier used in ASPM method, which can greatly improve the subpixel mapping performance. JHHS method applies supervised classification to the upsampled LR HSI with JCR-based classifier, to produce an HR classification map. This HR classification map is then integrated with the subpixel mapping result produced by JASPM method with decision fusion, to generate the final subpixel mapping result. Basically, supervised classification techniques other than JCRT-based classifier can also be used in both JASPM and CRSPM methods. Therefore, besides JCRT-based classifier, both SVM and JCR based classifiers are also employed in comparison experiment.

Subpixel mapping results and performance of different methods using various supervised classifiers for both data sets are depicted and evaluated in Figs. 4–7 and Tables III–VI. It is notable that, all the compared methods can be divided into one-branch methods (including ASPM, JASPM, and InHASPM methods) and two-branch methods (including ACSPM, CR-SPM, and HASPM methods) according to their framework structure. In one-branch methods, subpixel mapping results are directly obtained from the LR HSI. While in two-branch methods, either a real auxiliary HR image (in ACSPM method) or an artificial one (in CRSPM and HASPM methods) is used to improve the initial subpixel mapping results obtained by the corresponding one-branch methods. To make a fair evaluation, comparison is made among methods belonging to the same category (one-branch or two-branch).

Tables III and IV report the classification performance of different methods with the SVM-based classifier. For one-branch methods, the proposed InHASPM method remarkably

TABLE V
PERFORMANCE EVALUATION MEASUREMENTS OF DIFFERENT METHODS ON PAVIA UNIVERSITY DATA SET WITH JCR-BASED CLASSIFIER

Overall performance of one-branch methods					
Measurement	S1-InHASPM	S2-InHASPM	S3-InHASPM	JASPM	JASPM-JCRT
OA[%]	**90.70**	89.94	90.54	86.97	87.87
κ	**0.878**	0.869	0.876	0.830	0.843
APA[%]	**89.11**	88.82	89.06	85.78	87.61
AUA[%]	**87.06**	86.08	86.94	85.64	83.73
Time(s)	203.22	203.07	203.10	**166.73**	190.45
Overall performance of two-branch methods					
Measurement	S1-HASPM	S2-HASPM	S3-HASPM	CRSPM	CRSPM-JCRT
OA[%]	96.28	96.28	**96.31**	88.36	92.04
κ	**0.951**	**0.951**	**0.951**	0.848	0.896
APA[%]	94.01	94.03	**94.06**	87.14	89.70
AUA[%]	94.44	94.44	**94.48**	89.85	90.48
Time(s)	255.62	**255.40**	255.71	794.84	846.56

The bold entities indicate the best results and the underlined entities indicate the second best results.

TABLE VI
PERFORMANCE EVALUATION MEASUREMENTS OF DIFFERENT METHODS ON INDIAN PINES DATA SET WITH JCR-BASED CLASSIFIER

Overall performance of one-branch methods					
Measurement	S1-InHASPM	S2-InHASPM	S3-InHASPM	JASPM	JASPM-JCRT
OA[%]	94.83	94.94	**95.03**	93.59	93.04
κ	0.941	0.942	**0.943**	0.927	0.921
APA[%]	94.23	94.10	**94.27**	90.14	91.68
AUA[%]	92.52	92.39	92.65	**93.16**	90.39
Time(s)	54.26	54.38	54.20	**32.23**	37.35
Overall performance of two-branch methods					
Measurement	S1-HASPM	S2-HASPM	S3-HASPM	CRSPM	CRSPM-JCRT
OA[%]	96.14	96.02	**96.15**	95.48	95.74
κ	**0.956**	0.955	**0.956**	0.948	0.951
APA[%]	96.00	94.73	**96.34**	93.43	94.09
AUA[%]	95.77	95.64	94.76	**95.82**	95.19
Time(s)	82.16	82.22	**82.06**	300.63	308.78

The bold entities indicate the best results and the underlined entities indicate the second best results.

outperforms the others, especially for Pavia University data set, approximately 6% and 3% improvement in OA over ASPM and JASPM methods are obtained. Furthermore, Tables V and VI report the classification performance of different methods with the JCR-based classifier, InHASPM method also surpasses the others, especifically for Pavia University data set, nearly 4% and 3% improvement in OA over JASPM method and JASPM-JCRT method (JASMP method with JCRT-based classifier) are obtained. It can be observed that, among one-branch methods, the proposed InHASPM method clearly outperforms the others, by exhibiting much less misclassification. This improvement can be attributed to the adopted labeled-unlabeled hybrid endmember library and abundance optimization, since an abundance map with higher accuracy leads to a more accurate subpixel mapping result. While the improved accuracy comes at the cost of longer calculation time.

Among two-branch methods, the proposed HASPM method also clearly outperforms. The introduction of segmentation map of upsampled LR HSI as guideline provides further improvement in subpixel mapping accuracy, by incorporating spatial contextual information effectively. In Tables III–VI, the proposed HASPM method remarkably outperforms, especially for Pavia University data set, where approximate 13% and 10% improvement in OA over ACSPM and CRSPM methods can be obtained with SVM-based classifier, and with JCR-based classifier, approximate 8% and 4% improvement in OA over CRSPM method and CRSPM-JCRT method (CRSPM method with JCRT-based classifier) can be obtained. It is interesting to find out that when more advanced (of course more complicated) classifier (JCR-based classifier) is employed, the proposed HASPM method exhibits higher calculation efficiency than the others. It is also notable that two-branch methods normally lead to better performance than the corresponding one-branch methods by incorporating spatial contextual information.

The experimental results also illustrate that the proposed HASPM method seems less dependent on supervised classifiers employed. With SVM-based classifier and JCR-based one, comparable subpixel mapping results are produced: approximate evaluation measurements are obtained for Pavia University data set, and less than 3% difference can be observed in OA for Indian

Pines data set. While the performance of CRSPM method is highly dependent on the adopted supervised classifier, in which more advanced classifier (JCRT-based classifier > JCR-based classifier > SVM-based classifier) leads to better subpixel mapping performance. This merit of the proposed HASPM method can be attributed to the labeled-unlabeled hybrid endmember library and abundance optimization strategies adopted, which greatly improves the accuracy of abundance estimation and hence greatly improves the accuracy of subpixel mapping, even when the supervised classification is less accurate.

IV. Conclusion

A new subpixel mapping method (called HASPM) is proposed to deal with subpixel level classification of LR HSI. A hybrid labeled-unlabeled endmember library is constructed by training samples and unsupervised cluster centers of LR HSI. Abundance optimization strategies are employed to obtain an abundance map of LR HSI with improved accuracy. With the optimized fractional abundances, a subpixel mapping result is obtained using SPSAM. To further improve the subpixel mapping accuracy, spatial contextual information is incorporated by using unsupervised segmentation result of the upsampled LR HSI as guidelines for decision fusion. The experimental results demonstrate that the proposed HASPM method remarkably outperforms some state-of-the-art subpixel mapping methods both visually and quantitatively. It is also illustrated that, the proposed HASPM method is less dependent on supervised classifier adopted, which makes it quite competitive in practical applications.

References

[1] J. M. Bioucas-Dias, A. Plaza, G. Camps-Valls, P. Scheunders, N. M. Nasrabadi, and J. Chanussot, "Hyperspectral remote sensing data analysis and future challenges," *IEEE Geosci. Remote Sens. Mag.*, vol. 1, no. 2, pp. 6–36, Jun. 2013.

[2] G. Camps-Valls, D. Tuia, L. Bruzzone, and J. A. Benediktsson, "Advances in hyperspectral image classification," *IEEE Signal Process. Mag.*, vol. 31, no. 1, pp. 45–54, Jan. 2014.

[3] J. M. Bioucas-Dias *et al.*, "Hyperspectral unmixing overview: geometrical, statistical, and sparse regression-based approaches," *IEEE J. Sel. Topics Appl. Earth Observ. Remote Sens.*, vol. 5, no. 2, pp. 354–379, Apr. 2012.

[4] H. Zhu, "Linear spectral unmixing assisted by probability guided and minimum residual exhaustive search for subpixel classification," *Int. J. Remote Sens.*, vol. 26, no. 24, pp. 5585–5601, 2005.

[5] J. Boardman, "Automating spectral unmixing of AVIRIS data using convex geometry concepts," in *Proc. Ann. JPL Airborne Geosci. Workshop*, 1993, vol. 1, pp. 11–14.

[6] J. Nascimento and J. Bioucas-Dias, "Vertex component analysis: A fast algorithm to unmix hyperspectral data," *IEEE Trans. Geosci. Remote Sens.*, vol. 43, no. 4, pp. 898–910, Apr. 2005.

[7] C. I. Chang, C. C. Wu, W. Liu, and Y. C. Ouyang, "A new growing method for simplex-based endmember extraction algorithm," *IEEE Trans. Geosci. Remote Sens.*, vol. 44, no. 10, pp. 2804–2819, Oct. 2006.

[8] R. A. Neville, K. Staenz, T. Szeredi, J. Lefebvre, and P. Hauff, "Automatic endmember extraction from hyperspectral data for mineral exploration," in *Proc. Can. Symp. Remote Sens.*, 1999, pp. 21–24.

[9] M. E. Winter, "N-FINDR: An algorithm for fast autonomous spectral endmember determination in hyperspectral data," *Proc. SPIE*, vol. 3753, pp. 266–277, 1999.

[10] A. Villa, J. Chanussot, J. A. Benediktsson, and C. Jutten, "Spectral unmixing for the classification of hyperspectral images at a finer spatial resolution," *IEEE J. Sel. Topics Signal Process.*, vol. 5, no. 3, pp. 521–533, Jun. 2011.

[11] X. Lu, J. Zhang, T. Li, and Y. Zhang, "A novel synergetic classification approach for hyperspectral and panchromatic images based on self-learning," *IEEE Trans. Geosci. Remote Sens.*, vol. 54, no. 8, pp. 4917–4928, Aug. 2016.

[12] I. Dópido, J. Li, P. Gamba, and A. Plaza, "A new hybrid strategy combining semisupervised classification and unmixing of hyperspectral data," *IEEE J. Sel. Topics Appl. Earth Observ. Remote Sens.*, vol. 7, no. 8, pp. 3619–3629, Aug. 2014.

[13] J. Li, I. Dópido, P. Gamba, and A. Plaza, "Complementarity of discriminative classifiers and spectral unmixing techniques for the interpretation of hyperspectral images," *IEEE Trans. Geosci. Remote Sens.*, vol. 53, no. 5, pp. 2899–2912, May 2015.

[14] L. Zhang, Q. Zhang, B. Du, X. Huang, Y. Tang, and D. Tao, "Simultaneous spectral-spatial feature selection and extraction for hyperspectral images," *IEEE Trans. Cybern.*, vol. 48, no. 1, pp. 16–28, Jan. 2018.

[15] L. Zhang, L. Zhang, B. Du, J. You, and D. Tao, "Hyperspectral image unsupervised classification by robust manifold matrix factorization," *Inf. Sci.*, vol. 485, pp. 154–169, Jun. 2019.

[16] G. Tao, Z. Liu, J. Cao, and S. Liang, "Local difference ternary sequences descriptor based on unsupervised min redundancy mutual information feature selection," *Multidimensional Syst. Signal Process.*, vol. 31, no. 14, pp. 771–791, Jun. 2018.

[17] M. Ma, S. Mei, S. Wan, J. Hou, Z. Wang, and D. Feng, "Video summarization via block sparse dictionary selection," *Neorocomputing*, vol. 378, pp. 197–209, 2020.

[18] D. C. Heinz and C.-I. Chang, "Fully constrained least squares linear spectral mixture analysis method for material quantification in hyperspectral imagery," *IEEE Trans. Geosci. Remote Sens.*, vol. 39, no. 3, pp. 529–545, Mar. 2001.

[19] J. Boardman, "Leveraging the high dimensionality of AVIRIS data for improved subpixel target unmixing and rejection of false positives: Mixture tuned matched filtering," in *Proc. 5th JPL Geosci. Workshop*, 1998, pp. 55–56.

[20] N. Keshava and J. F. Mustard, "Spectral unmixing," *IEEE Signal Process. Mag.*, vol. 19, no. 1, pp. 44–57, Jan. 2002.

[21] P. M. Atkinson, "Mapping subpixel boundaries from remotely sensed images," in *Innovations in GIS 4*, vol. 4, London, U.K.: Taylor & Francis, 1997, pp. 166–180.

[22] W. R. Tobler, "A computer movie simulating urban growth in the detroit region," *Econ. Geography*, vol. 46, pp. 234–240, Jun. 1970.

[23] X. Xu, Y. Zhong, and L. Zhang, "A sub-pixel mapping method based on an attraction model for multiple shifted remotely sensed images," *Neurocomputing*, vol. 134, pp. 79–91, 2014.

[24] X. Tong, X. Zhang, J. Shan, H. Xie, and M. Liu, "Attraction-repulsion model-based subpixel mapping of multi-/hyperspectral imagery," *IEEE Trans. Geosci. Remote Sens.*, vol. 51, no. 5, pp. 2799–2814, May 2013.

[25] K. C. Mertens, B. De Baets, L. Verbeke, and R. De Wul, "A sub-pixel mapping algorithm based on sub-pixel/pixel spatial attraction models," *Int. J. Remote Sens.*, vol. 27, no. 15, pp. 3293–3310, Aug. 2006.

[26] C. Huang, Y. Chen, and J. Wu, "DEM-based modification of pixelswapping algorithm for enhancing floodplain inundation mapping," *Int. J. Remote Sens.*, vol. 35, pp. 365–381, 2014.

[27] P. M. Atkinson, "Sub-pixel target mapping from soft-classified, remotely sensed imagery," *Photogrammetry Eng. Remote Sens.*, vol. 71, no. 7, pp. 839–846, Jul. 2005.

[28] Y. Xu and B. Huang, "A spatio-temporal pixel-swapping algorithm for subpixel land cover mapping," *IEEE Geosci. Remote Sens. Lett.*, vol. 11, no. 2, pp. 474–478, Feb. 2014.

[29] Y. F. Su, G. M. Foody, A. M. Muad, and K. S. Cheng, "Combining pixel swapping and contouring methods to enhance super-resolution mapping," *IEEE J. Sel. Topics Appl. Earth Observ. Remote Sens.*, vol. 5, no. 5, pp. 1428–1437, Oct. 2012.

[30] X. Li, F. Ling, Y. Du, Q. Feng, and Y. Zhang, "A spatial-temporal hopfield neural network approach for super-resolution land cover mapping with multi-temporal different resolution remotely sensed images," *ISPRS J. Photogrammetry Remote Sens.*, vol. 93, pp. 76–87, 2014.

[31] A. J. Tatem, H. G. Lewis, P. M. Atkinson, and M. S. Nixon, 'Super resolution target identification from remotely sensed images using a hopfield neural network," *IEEE Trans. Geosci. Remote Sens.*, vol. 39, no. 4, pp. 781–796, Apr. 2001.

[32] Y. F. Zhong, Y. Y. Wu, X. Xu, and L. P. Zhang, "An adaptive subpixel mapping method based on map model and class determination strategy for hyperspectral remote sensing imagery," *IEEE Trans. Geosci. Remote Sens.*, vol. 53, no. 3, pp. 1411–1426, Mar. 2015.

[33] Y. F. Zhong, Y. Y. Wu, L. P. Zhang, and X. Xu, "Adaptive MAP subpixel mapping model based on regularization curve for multiple shifted hyperspectral imagery," *ISPRS J. Photogramm. Remote Sens.*, vol. 96, pp. 134–148, 2014.
[34] X. Xu, Y. Zhong, L. Zhang, and H. Zhang, "Sub-pixel mapping based on a MAP model with multiple shifted hyperspectral imagery," *IEEE J. Sel. Topics Appl. Earth Observ. Remote Sens.*, vol. 6, no. 2, pp. 580–593, Apr. 2013.
[35] X. Xu, Y. Zhong, and L. Zhang, "Adaptive sub-pixel mapping based on a multiagent system for remote sensing imagery," *IEEE Trans. Geosci. Remote Sens.*, vol. 52, no. 2, pp. 787–804, Feb. 2014.
[36] C. Zhao, W. Liu, Y. Wang, and X. Li, "Modified genetic algorithm-based sub-pixel mapping," *Optik*, vol. 125, pp. 6379–6383, 2014.
[37] L. Li, Y. Chen, T. Xu, R. Liu, K. Shi, and C. Huang, "Super-resolution mapping of wetland inundation from remote sensing imagery based on integration of back-propagation neural network and genetic algorithm," *Remote Sens. Environ.*, vol. 164, pp. 142–154, Jul. 2015.
[38] K. C. Mertens, L. P. C. Verbeke, E. I. Ducheyne, and R. R. D.Wulf,"Using genetic algorithms in sub-pixel mapping," *Int. J. Remote Sens.*, vol. 24, no. 21, pp. 4241–4247, Nov. 2003.
[39] Y. Zhong and L. Zhang, "Remote sensing image sub-pixel mapping based on adaptive differential evolution," *IEEE Trans. Syst., Man, Cybern. B, Cybern.*, vol. 42, no. 5, pp. 1306–1329, Oct. 2012.
[40] X. Xu, X. Tong, A. Plaza, Y. Zhong, H. Xie, and L. Zhang, "Using linear spectral unmixing for subpixel mapping of hyperspectral imagery: A quantitative assessment," *IEEE J. Sel. Topics Appl. Earth Observ. Remote Sens.*, vol. 10, no. 4, pp. 1589–1600, Apr. 2017.
[41] Z. Mahmood, M. A. Akhter, G. Thoonen, and P. Scheunders, "Contextual subpixel mapping of hyperspectral images making use of a high resolution color image," *IEEE J. Sel. Topics Appl. Earth Observ. Remote Sens.*, vol. 6, no. 2, pp. 779–791, Apr. 2013.
[42] Y. Zhang, X. Xue, T. Wang, and M. He, "A hybrid supixel mapping framework for hyperspectral image using collaborative representation," *IEEE J. Sel. Topics Appl. Earth Observ. Remote Sens.*, vol. 10, no. 11, pp. 5073–5086, Nov. 2017.
[43] F. Melgani and L. Bruzzone, "Classification of hyperspectral remote sensing images with support vector machines," *IEEE Trans. Geosci. Remote Sens.*, vol. 42, no. 8, pp. 1778–1790, Aug. 2004.
[44] B. Wohlberg, D. M. Tartakovsky, and A. Guadagnini, "Subsurface characterization with support vector machines," *IEEE Trans. Geosci. Remote Sens.*, vol. 44, no. 1, pp. 47–57, Jan. 2006.
[45] A. Mathur and G. M. Foody, "Multiclass and binary SVM classification: Implications for training and classification users," *IEEE Geosci. Remote Sens. Lett.*, vol. 5, no. 2, pp. 241–245, Apr. 2008.
[46] G. Mountrakis, J. Im, and C. Ogole, "Support vector machines in remote sensing: A review," *ISPRS J. Photogrammetry Remote Sens.*, vol. 66, no. 3, pp. 247–259, May 2011.
[47] W. Li, E. W. Tramel, S. Prasad, and J. E. Fowler, "Nearest regularized subspace for hyperspectral classification," *IEEE Trans. Geosci. Remote Sens.*, vol. 52, no. 1, pp. 477–489, Jan. 2014.
[48] W. Li and Q. Du, "Joint within-class collaborative representation for hyperspectral image classification," *IEEE J. Sel. Topics Appl. Earth Observ. Remote Sens.*, vol. 7, no. 6, pp. 2200–2208, Jun. 2014.

Yifan Zhang (Member, IEEE) received the B.S. degree in electron and information technology and the M.S. and Ph.D. degrees in signal and information processing from Northwestern Polytechnical University, Xi'an, China, in 2001, 2004, and 2007, respectively.

From 2007 to 2010, she worked as a Postdoctoral Researcher with the Vision Lab, Department of Physics, University of Antwerp, Antwerp, Belgium. She is currently an Associate Professor with the School of Electronics and Information, Northwestern Polytechnical University of China, Xi'an, China. Her research interest includes HSI analysis, image fusion, and restoration.

Ting Wang received the B.S. degree in electronic information science and technology from the School of Physics and Electronic Sciences, Shanxi Datong University, Datong, China, in 2015, and the M.S. degree in signal and information processing from the School of Electronics and Information, Northwestern Polytechnical University, Xi'an, China, in 2018.

Her major research interests include subpixel level analysis and processing of HSI.

Shaohui Mei (Member, IEEE) received the B.S. degree in electronics and information engineering and the Ph.D. degree in signal and information processing from Northwestern Polytechnical University, Xi'an, China, in 2005 and 2011, respectively.

He was a Visiting Student with the University of Sydney, Sydney, NSW, Australia from 2007 to 2008. He is currently an Associate Professor with the School of Electronics and Information, Northwestern Polytechnical University. His research interests include hyperspectral remote sensing image processing and applications, intelligent signal and information acquisition and processing, neural networks, pattern recognition, and machine learning.

Qian Du (Fellow, IEEE) received the Ph.D. degree in electrical engineering from the University of Maryland at Baltimore County, Baltimore, MD, USA, in 2000.

She is currently the Bobby Shackouls Professor with the Department of Electrical and Computer Engineering, Mississippi State University, Mississippi State, MS, USA. Her research interests include hyperspectral remote sensing image analysis and applications, pattern classification, data compression, and neural networks.

Dr. Du is a Fellow of IEEE and the SPIE-International Society for Optics and Photonics. She was a recipient of the 2010 Best Reviewer Award from the IEEE Geoscience and Remote Sensing Society. She was a Co-Chair for the Data Fusion Technical Committee of the IEEE Geoscience and Remote Sensing Society from 2009 to 2013, and the Chair for Remote Sensing and Mapping Technical Committee of the International Association for Pattern Recognition from 2010 to 2014. She served as an Associate Editor for the IEEE JOURNAL OF SELECTED TOPICS IN APPLIED EARTH OBSERVATIONS AND REMOTE SENSING, the Journal of Applied Remote Sensing, and the IEEE SIGNAL PROCESSING LETTER. Since 2016, she has been the Editor-in-Chief for the IEEE JOURNAL OF SELECTED TOPICS IN APPLIED EARTH OBSERVATIONS AND REMOTE SENSING. She is the General Chair for the 4th IEEE GRSS Workshop on HSI and Signal Processing: Evolution in Remote Sensing in Shanghai, China, in 2012.